

Linear Magnetoresistance and Anomalous Hall Effect in the Superconductor NiBi₃

Gabriel Sant'ana,^{*} Jully Paola Peña Pacheco, David Mockli, Fabiano Mesquita

da Rosa, Sergio Garcia Magalhães, Paulo Pureur, and Milton A. Tumelero[†]

Instituto de Física, Universidade Federal do Rio Grande do Sul, 91501-970 Porto Alegre, Brazil

(Dated: June 15, 2025)

The NiBi₃ compound exhibits an intriguing interplay of superconductivity, magnetism, and topology. While the possibility of unconventional superconductivity involving magnetic interactions has been previously discussed and dismissed, the topological character of its electronic structure has only recently gained attention. Here, we report experimental evidence of unconventional magnetic ordering in high-quality single crystals of NiBi₃, revealed through detailed magnetotransport measurements. The magnetoresistance shows a distinct temperature dependence, combining a classical Lorentz-like component with a linear-in-field contribution. Moreover, anomalous Hall effect signals persist down to the superconducting transition and vanish above 75 K. These results indicate that spin textures significantly influence charge transport in NiBi₃, pointing to a compensated magnetic background intertwined with its topological electronic structure. Our findings underscore the complex and multifaceted nature of this material.

The interplay between superconductivity, magnetism, and topology has driven the discovery of several emergent electronic phases. Some of these states offer potential for future energy and information technologies through the development of magnetic and topological superconductors, as well as spintronic devices [1]. Superconductors containing 3d magnetic elements are of particular interest, as magnetic correlations often compete with the superconducting pairing mechanism. The intermetallic compound NiBi₃ is a type-II superconductor with strong electron-phonon coupling and a critical temperature of approximately 4 K [2, 3]. Early studies suggested coexistence of ferromagnetism (FM) and superconductivity due to magnetization observed below the critical temperature [4, 5]. However, more accurate investigations on the magnetization of single crystals ruled out long-range FM order and spontaneous magnetization in this system [6, 7]. Nevertheless, electron spin resonance signals were detected up to 150 K, indicating the presence of magnetic fluctuations [8] and keeping open the prospect of unconventional or compensated magnetic order in this compound.

Recent studies combining density functional theory and angle-resolved photoemission spectroscopy (ARPES) revealed topological surface states in Bi₃Ni [9, 10]. Although topological superconductivity was ruled out—since the surface bands lie far below the Fermi energy, additional features such as nodal lines and nodal surfaces highlight this compound as a platform for emergent phenomena and potential applications.

Separately, epitaxial Ni/Bi bilayers have demonstrated signatures of time-reversal symmetry breaking and chiral p-wave superconductivity [11–17]. In these systems, the spontaneous formation of NiBi₃ at the interface appears to play a central role in the onset of superconductivity [18–22]. Indeed, the role of NiBi₃ has been identified

as critical to the development of unconventional pairing mechanisms [21, 23]. However, several microscopic studies on pure NiBi₃—including muon spin rotation [6], Andreev reflection spectroscopy [24], and Kerr rotation experiments [7] have consistently established conventional s-wave superconductivity [25].

Despite this recent progress, the normal-state magnetic and electronic properties of NiBi₃ remain largely unexplored. The confirmation of a magnetic ordering could be an outstanding result, in addition to the nontrivial topology, to a complete description of NiBi₃ properties and superconductivity. Here, we investigate its magnetotransport behavior using high-quality single crystals. Our results reveal an unconventional magnetoresistance that is linear in magnetic field at low fields and increases linearly with temperature. Moreover, we report the first Hall effect measurements for this compound, which display a substantial anomalous contribution. Together, our findings point to a time-reversal symmetry-broken electronic state in NiBi₃ characterized by a compensated spin texture.

Needle-like NiBi₃ samples were prepared by the self-flux method using a component ratio of Bi₁₀:Ni₁. High-purity Bi (99.999%) and Ni (99.99%) powders were sealed in a vacuum quartz ampule, heated to 1140°C, and subjected to a two-step cooling process: initially cooled from 1250°C to 740°C at a rate of 3°C/min, followed by slow cooling to 580°C at 1.6°C/h. Single crystals were separated from the flux by centrifugation. Figure 1b shows a representative needle-like crystal with approximate dimensions of 2 mm × 0.1 mm × 0.1 mm. Grazing incidence X-ray diffraction (GIXRD) measurements were carried out using Cuα₁ radiation to determine phase purity and crystallographic orientation. Magnetotransport measurements were performed using a home-built setup equipped with a CMag9 cryostat (Cryomagnetics), employing the standard four-probe method. The electrical current was applied along the crystallographic *b*-axis.

Fig. 1a shows the GIXRD pattern obtained from a batch of NiBi₃ single crystals. The diffraction peaks cor-

^{*} gabriel.santana.dasilva@outlook.com

[†] matumelero@if.ufrgs.br

respond to the orthorhombic NiBi_3 phase with $Pnma$ symmetry, as indexed in the figure. No secondary or segregated phases were detected in the XRD analysis. Furthermore, all crystals were aligned along the b -axis, as evidenced by the exclusive observation of reflections with $k = 0$ in the Miller index, confirming preferential needle growth along the crystallographic b -direction.

The atomic structure of NiBi_3 is illustrated schematically in Fig. 1c. NiBi_3 consists of long quasi-one-dimensional chains running along the b -axis. The unit cell contains two such chains, each comprising two Ni atoms. These chains are not equivalent: one is rotated relative to the other by approximately 25° about the b -axis. Despite the structural quasi-1D character, the valence bands exhibit significant dispersion in energy [10].

Fig. 1d presents the temperature dependence of the longitudinal resistivity (ρ_{xx}) for three different NiBi_3 single crystals. The observed profiles are consistent with previous reports for this material system, featuring early resistivity saturation, a superconducting transition near 4 K (see inset of Fig. 1d), and a residual resistivity ratio (RRR) in line with the literature [3, 6–8, 26]. The residual resistivity values (ρ_0) were measured as 12.7, 11.2, and 12.1 $\mu\Omega\cdot\text{cm}$ for samples S1, S2, and S3, respectively, yielding RRRs (defined as $\rho(300\text{ K})/\rho_0$) of 18.1, 20.7, and 20.1. All samples exhibit sharp superconducting transitions with widths below 300 mK.

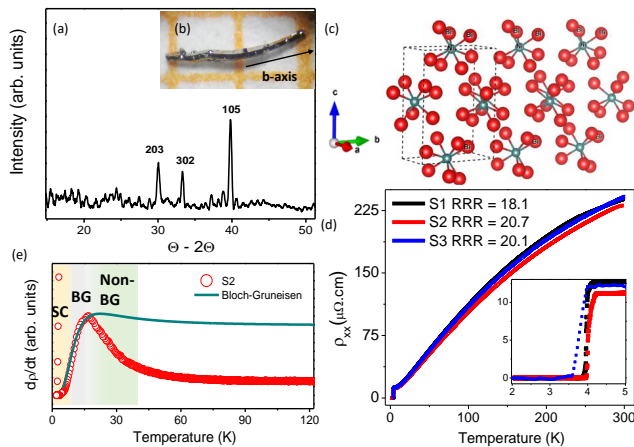


FIG. 1. (a) GIXRD diffractogram from several NiBi_3 needle-like single crystals. (b) Photograph of a single crystal. (c) Side view of the orthorhombic NiBi_3 structure. (d) Temperature-dependent resistivity for samples S1, S2, and S3. *Inset*: Zoom-in of the superconducting transition. (e) First derivative of resistivity with respect to temperature for sample S2. Solid lines represent simulations using the Bloch–Grüneisen (BG) model.

Fig. 1e shows the resistivity derivative for sample S2; results for other samples are provided in the Supplementary Material (SM). From 5 K to 15 K, the resistivity follows the standard Bloch–Grüneisen (BG) behavior, described by:

$$\rho_{BG}(T) = \rho_0 + A \left(\frac{T}{\Theta_D} \right)^5 \int_0^{\Theta_D/T} \frac{x^5 dx}{(e^x - 1)(1 - e^{-x})}, \quad (1)$$

where Θ_D is the Debye temperature and A is a material-dependent constant. The BG model accounts for carrier scattering by acoustic phonons. The simulated curve is shown alongside the experimental data in Fig. 1e (grey-shade region). A fit yields $\Theta_D \approx 65$ K, consistent with previous experimental estimates [8, 26].

According to the BG model, the first derivative of resistivity initially increases as T^4 , followed by a maximum corresponding to the crossover where phonon population becomes significant. Beyond this point, the derivative slightly decreases and reaches a plateau, marking the regime where electron-phonon scattering saturates. In our experimental data, the maximum in $d\rho/dT$ occurs near 16 K for sample S2. Above this temperature, however, the derivative decays exponentially, deviating from BG predictions (green-shaded region in Fig. 1e). This deviation strongly suggests an additional scattering mechanism beyond electron-phonon coupling. To date, the resistivity behavior in NiBi_3 has been modeled using various approaches, such as parallel resistor models [26, 34], exponential terms [8, 35], and Bloch–Grüneisen functions [6] to account for the early resistivity saturation. However, a microscopic description of the transport mechanism remains unresolved.

Fig. 2a shows transversal resistivity measurements (ρ_{xy}) in NiBi_3 , which clearly exhibit anomalous Hall effect (AHE) characteristics. The S-shaped ρ_{xy} versus H curves reflect the anomalous behavior: while ρ_{xy} saturates at high fields (ordinary Hall regime), it reverses abruptly near zero field. The anomalous Hall resistivity ρ_{AHE} is extracted by extrapolating the linear high-field region to zero field. At low temperatures, ρ_{AHE} is approximately 25 $\text{n}\Omega\cdot\text{cm}$, increasing to around 220 $\text{n}\Omega\cdot\text{cm}$ near 75 K. Above 150 K and up to 300 K, the AHE decreases strongly, almost vanishing. The temperature dependence of ρ_{AHE} is summarized in Fig. 2b, while Fig. 2c displays the natural $\ln(\rho_{AHE})$ vs $\ln(\rho_{xx})$ plot, indicating a linear scaling from the $\rho_{AHE} \propto \rho_{xx}^\beta$ relation.

The AHE is typically associated with broken time-reversal symmetry (TRS) [37]. FM is the most common source of TRS breaking due to uncompensated magnetic moments. Nonetheless, the presence of long-range FM order in NiBi_3 has been extensively ruled out [3, 8]. Indeed, our magnetization measurements using a SQUID magnetometer confirm the absence of spontaneous magnetization (see SM, Fig. SM2, showing FC and ZFC curves under various magnetic fields). Notably, AHE has also been reported in compensated spin systems such as altermagnets [39–41] and non-collinear antiferromagnets [42], where ρ_{AHE} emerges despite a net-zero magnetic moment. The extinction of AHE between 75 and 150 K may reflect a Néel-like transition in a compensated magnetic phase. Furthermore, the observed linear scaling of ρ_{AHE} with ρ_{xx} ($\beta \approx 1$) is typical of magnetic systems and

is commonly attributed to skew-scattering mechanisms [37, 38]. A subtle feature in ρ_{xy} near zero field may also indicate additional scattering effects.

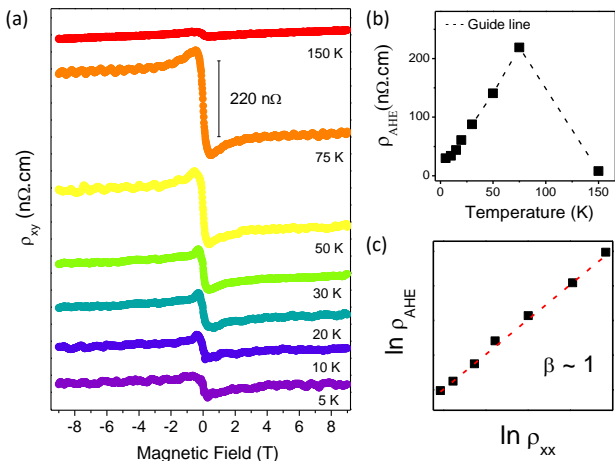


FIG. 2. Anomalous Hall effect in NiBi₃ (sample S3). (a) ρ_{xy} versus H at various temperatures. (b) ρ_{AHE} as a function of temperature; the gap between 80 and 140 K highlights the abrupt drop around 150 K. (c) \ln plot of ρ_{AHE} vs ρ_{xx} revealing the linear relation among the quantities.

Fig. 3a,b presents the magnetoresistance (MR), defined as $\Delta\rho(B)/\rho_0$, measured in the normal state with transverse magnetic field applied to the b -axis. Data for other samples are included in the SM (Fig. SM3). At 5 K and 10 K, MR exhibits a positive, parabolic-like behavior with positive curvature, consistent with orbital deflection of carriers. Above 20 K, MR remains positive but shows negative curvature and becomes linear at low fields. The MR magnitude initially decreases with temperature, reaching a minimum between 10 and 20 K, then increases again at higher temperatures. Fig. 3c summarizes the MR values for different samples and temperatures.

Kohler's plot for sample S1 is shown in Fig. 3d. At low temperatures, the curves collapse, obeying Kohler's rule (KR). However, at higher temperatures, KR is violated. The semiclassical KR relation assumes a single conduction channel with isotropic, field-independent scattering rates [29]:

$$\text{MR} = f(\omega_c\tau) = f\left(\frac{B}{\rho(0,T)}\right), \quad (2)$$

where ω_c is the cyclotron frequency, τ is the scattering time, and $\rho(0,T)$ is the zero-field resistivity. Deviations from KR in NiBi₃ have been previously reported [8]. In general, violations are attributed to multiband transport or anisotropic scattering. Although temperature-dependent carrier density (n_c) has been proposed as a possible cause [27], our data suggest otherwise. Specifically, the linear increase in MR above 20 K at low fields

(blue-shaded region in Fig. 3d) prevents any normalization that would collapse the curves onto those from lower temperatures. This suggests that changes in n_c are not the primary source of KR violation in NiBi₃. Interestingly, the temperature at which the MR behavior changes coincides with the maximum in $d\rho/dT$ (see Fig. 1e), reinforcing the presence of a secondary scattering mechanism.

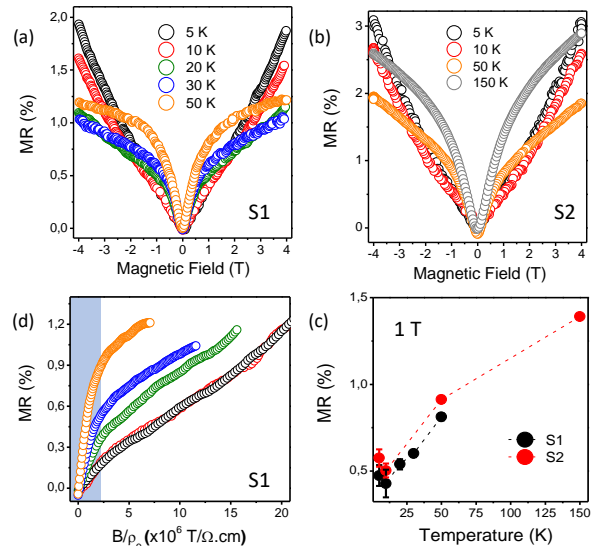


FIG. 3. Magnetoresistance (MR) in function of magnetic field for (a) S1 and (b) S2. (c) MR in function of temperature at 1 T for all samples. (d) Kohler's rule analysis for samples S1.

To further investigate the magnetotransport mechanism, we fitted the MR curves in two regimes: a quadratic component at high fields and a linear term at low fields. Fig. 4a illustrates the fitting procedure for sample S1 at 5 K and 50 K. The extracted quadratic coefficients were normalized at 5 K and are plotted in Fig. 4b as a function of temperature for samples S1, S2 and S3. These values reflect the ordinary MR, which scales as $\text{MR} \propto (\mu B)^2$, where μ is carrier mobility, typically inversely proportional to resistivity in metals. Dashed lines in Fig. 4b represent a $1/T$ trend, which agrees well with the quadratic coefficients, indicating that ordinary MR dominates at low temperatures and high fields.

The low-field linear MR coefficient (for $B < 1$ T) is shown in Fig. 4c, increasing with temperature for all samples. Notably, this coefficient scales linearly with the longitudinal resistivity, in contrast to the quadratic component, as revealed the inset of 4c. This behavior is unconventional and suggests a distinct transport mechanism. Based on this, we conclude that the overall increase in MR at higher temperatures is exclusively due to the linear mechanism.

The simultaneous presence of linear MR and AHE provides compelling evidence of magnetic ordering in NiBi₃. The linear MR, which scales with ρ_{xx} , is particularly unconventional and may be a signature of a compensated

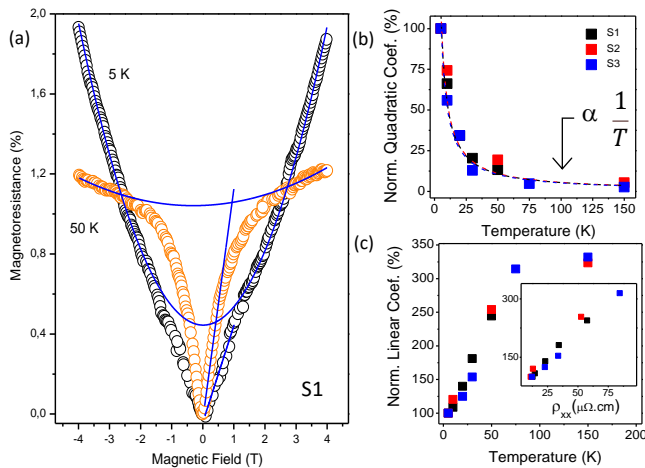


FIG. 4. (a) Fitting of MR into low-field linear and high-field quadratic components. (b) Quadratic coefficient normalized at 5 K vs. temperature for S1, S2, and S3. (c) Temperature-dependence of the linear coefficient normalized at 5 K. *Inset*: its correlation with ρ_{xx} .

spin texture. Curiously, the linear coefficient stop increasing above 75 K and reduces in 300 K, in agreement to AHE results. One possible explanation involves the two-spin-channel model proposed by Campbell and Fert [43], in which spin-flip processes open an additional conduction channel. Under an applied field, this channel is

suppressed, leading to an increase in resistivity. In this context, the observed linear MR merits further investigation. Additionally, the established topological features of NiBi_3 may also contribute to the unusual magnetotransport behavior observed. Finally, our data show that both the linear MR and AHE persist up to the superconducting transition, reviving the discussion on the conventional nature of superconductivity in this system now from the perspective of a compensated magnetic order.

In conclusion, the observation of the anomalous Hall effect and low-field linear magnetoresistance below 150 K provides strong evidence for a spin-compensated magnetic phase in NiBi_3 . These findings complement previous reports of magnetic fluctuations and topological features, contributing to the understanding of the complex electronic structure of this material. In particular, the linear magnetoresistance whose amplitude scales with the longitudinal resistivity appears to be intrinsically linked to an underlying magnetic order, highlighting an unconventional transport mechanism that warrants further investigation.

ACKNOWLEDGMENTS

The authors would like to acknowledge the funding agencies FAPERGS, CAPES and CNPq, in terms of the following grants: Pronex grant no. 16/0490-0 (Fapergs-CNPq)

-
- [1] J. Linder and J. W. Robinson, Superconducting spintronics, *Nature Physics* **11**, 307 (2015).
 - [2] J. Kumar, A. Kumar, A. Vajpayee, B. Gahtori, D. Sharma, P. Ahluwalia, S. Auluck, and V. Awana, Physical property and electronic structure characterization of bulk superconducting bi_3ni , *Superconductor Science and Technology* **24**, 085002 (2011).
 - [3] B. Silva, R. Luccas, N. Nemes, J. Hanko, M. Osorio, P. Kulkarni, F. Mompean, M. García-Hernández, M. Ramos, S. Vieira, *et al.*, Superconductivity and magnetism on flux-grown single crystals of nibi_3 , *Physical Review B—Condensed Matter and Materials Physics* **88**, 184508 (2013).
 - [4] E. L. M. Piñeiro, B. L. R. Herrera, R. Escudero, and L. Bucio, Possible coexistence of superconductivity and magnetism in intermetallic nibi_3 , *Solid state communications* **151**, 425 (2011).
 - [5] T. Herrmannsdörfer, R. Skrotzki, J. Wosnitzer, D. Köhler, R. Boldt, and M. Ruck, Structure-induced coexistence of ferromagnetic and superconducting states of single-phase bi_3ni seen via magnetization and resistance measurements, *Physical Review B—Condensed Matter and Materials Physics* **83**, 140501 (2011).
 - [6] T. Shang, J. Meng, X. Zhu, H. Zhang, B. Yu, Z. Zhen, Y. Wang, Y. Xu, Q. Zhan, D. J. Gawryluk, *et al.*, Fully gapped superconductivity with preserved time-reversal symmetry in nibi_3 single crystals, *Physical Review B* **107**, 174513 (2023).
 - [7] J. Wang, C. Farhang, D. Yue, X. Jin, X. Zhu, and J. Xia, Absence of spontaneous time-reversal symmetry breaking and ferromagnetism in superconducting nibi_3 single crystal, *Physical Review B* **107**, 024415 (2023).
 - [8] X. Zhu, H. Lei, C. Petrovic, and Y. Zhang, Surface-induced magnetic fluctuations in a single-crystal nibi_3 superconductor, *Physical Review B—Condensed Matter and Materials Physics* **86**, 024527 (2012).
 - [9] C. Adriano, K. Lee, Y. Kushnirenko, B. Schruck, K. R. Pakuszewski, L.-L. Wang, S. L. Bud'ko, P. C. Canfield, and A. Kaminski, Bulk and surface electronic structure of nibi_3 , *Physical Review B* **107**, 165107 (2023).
 - [10] J. Zhang, K.-Y. Jiang, S.-X. Qiao, P.-C. Xiao, N. Jiao, P. Zhang, H.-Y. Lu, and Q.-F. Liang, Nodal points, lines, and surfaces, and topological surface states in superconductor nibi_3 , *Phys. Rev. B* **111**, 094508 (2025).
 - [11] X.-X. Gong, H.-X. Zhou, P.-C. Xu, D. Yue, K. Zhu, X.-F. Jin, H. Tian, G.-J. Zhao, and T.-Y. Chen, Possible p-wave superconductivity in epitaxial bi/ni bilayers, *Chinese Physics Letters* **32**, 067402 (2015).
 - [12] X. Gong, M. Kargarian, A. Stern, D. Yue, H. Zhou, X. Jin, V. M. Galitski, V. M. Yakovenko, and J. Xia, Time-reversal symmetry-breaking superconductivity in epitaxial bismuth/nickel bilayers, *Science advances* **3**, e1602579 (2017).
 - [13] P. Chauhan, F. Mahmood, D. Yue, P.-C. Xu, X. Jin, and N. Armitage, Nodeless bulk superconductivity in the time-reversal symmetry breaking bi/ni bilayer system,

- Physical review letters **122**, 017002 (2019).
- [14] J. Wang, X. Gong, G. Yang, Z. Lyu, Y. Pang, G. Liu, Z. Ji, J. Fan, X. Jing, C. Yang, *et al.*, Anomalous magnetic moments as evidence of chiral superconductivity in a bi/ni bilayer, *Physical Review B* **96**, 054519 (2017).
- [15] H. Hayashi and K. Ando, Two-dimensional rashba superconductivity in ni/bi bilayers evidenced by non-reciprocal transport, *Applied Physics Reviews* **11**, 011401 (2024), https://pubs.aip.org/aip/apr/article-pdf/doi/10.1063/5.0158237/18283582/011401_1_5.0158237.pdf
- [16] R. Cai, D. Yue, W. Qiao, L. Guo, Z. Chen, X. C. Xie, X. Jin, and W. Han, Nonreciprocal transport of superconductivity in a bi/ni bilayer, *Phys. Rev. B* **108**, 064501 (2023).
- [17] J.-C. He and Y. Chen, Evidence of triplet superconductivity in bi/ni bilayers: Theoretical analysis of point contact andreev reflection spectroscopy results, *Phys. Rev. B* **106**, 224508 (2022).
- [18] M. Vaughan, N. Satchell, M. Ali, C. J. Kinane, G. B. Stenning, S. Langridge, and G. Burnell, Origin of superconductivity at nickel-bismuth interfaces, *Physical Review Research* **2**, 013270 (2020).
- [19] V. Siva, K. Senapati, B. Satpati, S. Prusty, D. Avasthi, D. Kanjilal, and P. K. Sahoo, Spontaneous formation of superconducting nibi₃ phase in ni-bi bilayer films, *Journal of Applied Physics* **117**, 083902 (2015).
- [20] G. Sant'ana, D. Möckli, A. d. C. Viegas, P. Pureur, and M. A. Tumelero, Ni/bi bilayers: The effect of thickness on the superconducting properties, *Journal of Applied Physics* **135** (2024).
- [21] J. Park, J. A. Horn, D. J. Kirsch, R. K. Pant, H. Yoon, S. Baek, S. Sarker, A. Mehta, X. Zhang, S. Lee, R. Greene, J. Paglione, and I. Takeuchi, Superconducting phase diagram in bi_xni_{1-x} thin films: The effects of bi stoichiometry on superconductivity, *Phys. Rev. Mater.* **8**, 074805 (2024).
- [22] S.-P. Chao, Superconductivity in a bi/ni bilayer, *Physical Review B* **99**, 064504 (2019).
- [23] L. Liu, Y. Xing, I. Merino, H. Micklitz, D. Franceschini, E. Baggio-Saitovitch, D. Bell, and I. Solórzano, Superconductivity in bi/ni bilayer system: Clear role of superconducting phases found at bi/ni interface, *Physical Review Materials* **2**, 014601 (2018).
- [24] G. Zhao, X. Gong, P. Xu, B. Li, Z. Huang, X. Jin, X.-D. Zhu, and T. Chen, Singlet superconductivity in a single-crystal nibi₃ superconductor, *Superconductor Science and Technology* **31**, 125005 (2018).
- [25] E. Gati, L. Xiang, L.-L. Wang, S. Manni, P. C. Canfield, and S. L. Bud'ko, Effect of pressure on the physical properties of the superconductor nibi₃, *Journal of Physics: Condensed Matter* **31**, 035701 (2018).
- [26] Y. Fujimori, S.-i. Kan, B. Shinozaki, and T. Kawaguti, Superconducting and normal state properties of nibi₃, *Journal of the Physical Society of Japan* **69**, 3017 (2000).
- [27] J. Xu, F. Han, T.-T. Wang, L. R. Thoutam, S. E. Pate, M. Li, X. Zhang, Y.-L. Wang, R. Fotovat, U. Welp, *et al.*, Extended kohler's rule of magnetoresistance, *Physical Review X* **11**, 041029 (2021).
- [28] S. Pate, B. Chen, B. Shen, K. Li, X. Zhou, D. Y. Chung, R. Divan, M. G. Kanatzidis, U. Welp, W.-K. Kwok, *et al.*, Extended kohler's rule of magnetoresistance in taco 2 te 2, *Physical Review B* **109**, 035129 (2024).
- [29] M. Kohler, Zur magnetischen widerstandsänderung reiner metalle, *Annalen der Physik* **424**, 211 (1938).
- [30] A. B. Pippard, *Magnetoresistance in metals*, Vol. 2 (Cambridge university press, 1989).
- [31] D. Woodard and G. Cody, Anomalous resistivity of nb 3 sn, *Physical Review* **136**, A166 (1964).
- [32] H. Wiesmann, M. Gurrvitch, H. Lutz, A. Ghosh, B. Schwarz, M. Strongin, P. Allen, and J. Halley, Simple model for characterizing the electrical resistivity in a- 15 superconductors, *Physical Review Letters* **38**, 782 (1977).
- [33] O. Gunnarsson, M. Calandra, and J. Han, Colloquium: Saturation of electrical resistivity, *Reviews of Modern Physics* **75**, 1085 (2003).
- [34] P. Nédélec, F. Creppy, L. Dumoulin, and J. Burger, Anomalous electrical resistivity of bi₃ni, *Physics Letters A* **111**, 67 (1985).
- [35] M. S. M. Sakurai, T. O. T. Ono, I. Y. I. Yoshida, and S. T. S. Tanuma, Thermoelectric and thermogalvanomagnetic properties of nibi₃, *Japanese Journal of Applied Physics* **39**, 6366 (2000).
- [36] T. Shang, J. Meng, X. Y. Zhu, H. Zhang, B. C. Yu, Z. X. Zhen, Y. H. Wang, Y. Xu, Q. F. Zhan, D. J. Gawryluk, and T. Shiroka, Fully gapped superconductivity with preserved time-reversal symmetry in nibi₃ single crystals, *Phys. Rev. B* **107**, 174513 (2023).
- [37] N. Nagaosa, J. Sinova, S. Onoda, A. H. MacDonald, and N. P. Ong, Anomalous hall effect, *Reviews of modern physics* **82**, 1539 (2010).
- [38] J. Smit, The spontaneous hall effect in ferromagnetics i, *Physica* **21**, 877 (1955).
- [39] L. Šmejkal, J. Sinova, and T. Jungwirth, Emerging research landscape of altermagnetism, *Phys. Rev. X* **12**, 040501 (2022).
- [40] T. Sato, S. Haddad, I. C. Fulga, F. F. Assaad, and J. van den Brink, Altermagnetic anomalous hall effect emerging from electronic correlations, *Phys. Rev. Lett.* **133**, 086503 (2024).
- [41] L. Attias, A. Levchenko, and M. Khodas, Intrinsic anomalous hall effect in altermagnets, *Phys. Rev. B* **110**, 094425 (2024).
- [42] L. Šmejkal, A. H. MacDonald, J. Sinova, S. Nakatsuji, and T. Jungwirth, Anomalous hall antiferromagnets, *Nature Reviews Materials* **7**, 482 (2022).
- [43] A. Fert and I. A. Campbell, Electrical resistivity of ferromagnetic nickel and iron based alloys, *Journal of Physics F: Metal Physics* **6**, 849 (1976).

SUPPLEMENTARY MATERIALS

First derivative of resistivity is shown in Fig. SM1 for S1 and S3. The divergence in the blue-shade region correspond to the superconducting transition. Above the critical temperature, both samples follows the standard Bloch-Gruneisen (BG) behavior, as indicated by the solid colored lines. The crossover in which phonon modes become thermally excited are represented by the peak in $d\rho/dT$. For S3, it manifest around 15 K, similar to S2 in the main text, while in S3, the peak appears at 30 K. After the maxima, decreasing of $d\rho/dT$ reflect a deviation from BG predictions of linear-scatter contribution. Such a deviation occurs smoothly for S3 and abruptly for S1, similar to S2. This difference is associated with

variation of the crystal size and shape, which is reflected by the difference in Debye temperature (Θ_D), being around 70 K for S1 and S2, and larger for S3 (85 K).

The first derivative of the resistivity with respect to temperature, $d\rho/dT$, is shown in Fig. SM1 for samples S1 and S3. The sharp divergence within the blue-shaded region corresponds to the superconducting transition. Above the critical temperature, both samples exhibit behavior consistent with the Bloch-Grüneisen (BG) model, as indicated by the solid colored lines. The temperature at which phonon modes become thermally activated—marked by the peak in $d\rho/dT$ indicates the crossover to dominant electron-phonon scattering. For S1, this peak occurs around 15 K, similar to the behavior of sample S2 discussed in the main text, while for S3 the peak appears near 30 K. Beyond the peak, the decrease in $d\rho/dT$ reflects a deviation from the linear temperature dependence predicted by the BG model. This deviation occurs smoothly for S3 but more abruptly for S1, again resembling the behavior observed in S2. The contrast is attributed to variations in crystal size and morphology, which affect the Debye temperature (Θ_D), estimated as 70 K for S1 and around 85 K for S3.

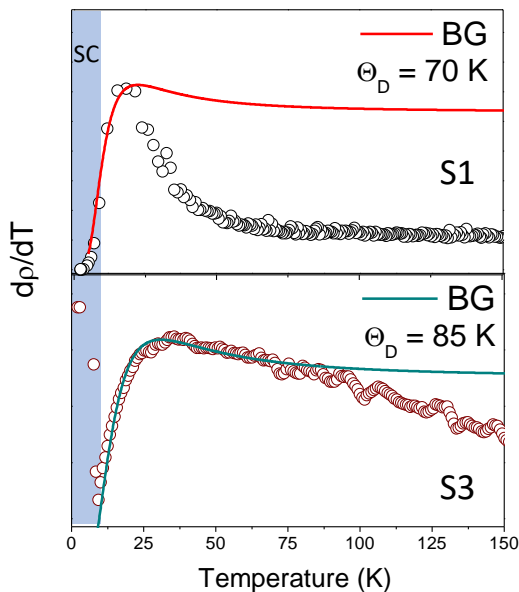


FIG. SM1. First derivative of resistivity for S1 and S3. Colored lines correspond to the simulation of Bloch-Grüneisen (BG) first derivative for a fixed Debye temperature (Θ_D). Blue-shaded region divergence is due to the superconducting (SC) transition.

Magnetization measurements were performed on a batch of NiBi_3 single crystals using a Superconducting Quantum Interference Device (SQUID) magnetometer

from Quantum Design. Fig. SM2a shows the DC magnetic susceptibility as a function of temperature under various applied magnetic fields. The upper branches correspond to field-cooled (FC) measurements, while the lower branches represent zero-field-cooled (ZFC) data. A noticeable bifurcation between FC and ZFC curves marks the onset of magnetic irreversibility, with the irreversibility temperature for each field indicated by dashed lines. Small oscillations with amplitudes on the order of 1×10^{-9} emu are attributed to minor variations in sample positioning during measurement and do not reflect intrinsic properties of the crystals. Fig. SM2b presents the magnetization as a function of temperature under an applied field of 500 Oe, clearly demonstrating the diamagnetic response of the sample.

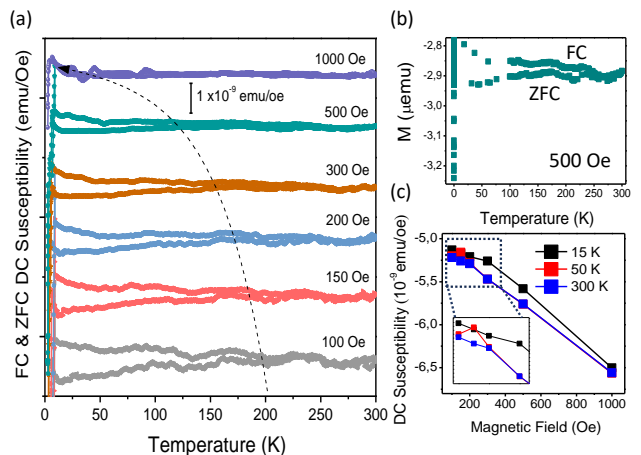


FIG. SM2. (a) DC susceptibility as a function of temperature under various magnetic fields for a batch of NiBi_3 single crystals. Field-cooled (FC) and zero-field-cooled (ZFC) measurements are shown. (b) Magnetization as a function of temperature at 500 Oe. (c) DC susceptibility as a function of magnetic field at 15 K, 50 K, and 300 K for FC measurements.

Magnetoresistance (MR) measurements as a function of magnetic field at various temperatures for sample S3 are shown in Fig. SM3a. The out-of-scale plots emphasize the evolution of the MR behavior. From 5 K to 15 K, the MR exhibits a purely quadratic dependence, consistent with ordinary MR mechanisms. At 20 K, a weak linear contribution begins to emerge and becomes increasingly prominent at higher temperatures. As shown in Fig. SM3b, where the MR at 2 T is plotted versus temperature, this linear component reaches a maximum around 75 K and subsequently diminishes. Consequently, as depicted in Fig. SM3c, the overall MR increases with temperature despite a suppression of the quadratic contribution, due to the dominance of the linear term at intermediate temperatures

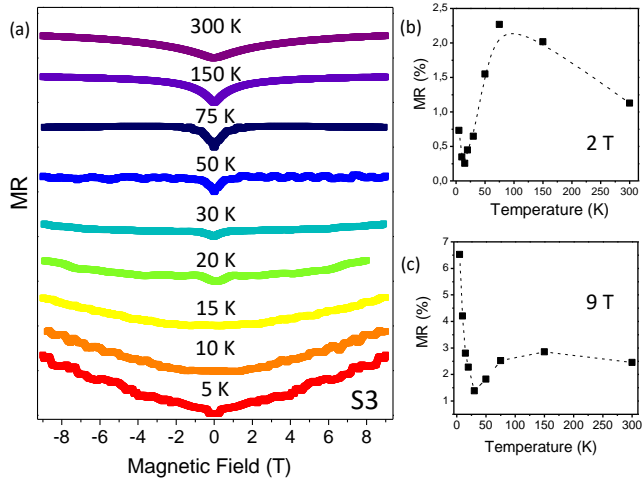


FIG. SM3. Magnetoresistance (MR) of sample S3. (a) Out-of-scale MR in function of magnetic field for several temperatures. MR values in function of temperature at (b) 2 T and (c) 9 T.